GA–A22091
CONF-950704--17

RECENT DIII–D DIVERTOR RESEARCH

by
S.L. ALLEN, A.S. BOZEK, N.H. BROOKS, D.A. BUCHENAUER, K.H. BURRELL, T.N. CARLSTROM, J.W. CUTHBERTSON, J.C. DeBOO, R. ELLIS, J.C. EVANS, T.E. EVANS, M.E. FENSTERMACHER, R.W. GEER, Ph. GHENDRIH, R.J. GROEBNER, D.N. HILL, D.L. HILLIS, J.T. HOGAN, M.A. HOLLERBACH, K.L. HOLTROP, C.L. HSIEH, A.W. HYATT, G.L. JACKSON, R.A. JAMES, W.R. JOHNSON, R. JONG, R. JUNGE, C.C. KLEPPER, C.J. LASNIER, G.J. LAUGHON, A.W. LEONARD, M.A. MAHDAVI, R. MAINGI, M.M. MENON, P.K. MIODUSZEWSKI, R.A. MOYER, W.H. MEYER, D.G. NILSON, T.H. OSBORNE, D.O. OVERSKEI, L.W. OWEN, T.W. PETRIE, D.A. PHELPS, G.D. PORTER, M.E. RENSINK, G.T. SAGER, M.J. SCHAFFER, K.M. SCHAUBEL, T.C. SIMONEN, J.P. SMITH, G.M. STAEBLER, R.D. STAMBAUGH, R.E. STOCKDALE, D.M. THOMAS, M.R. WADE, J.G. WATKINS, F. WESCHENFELDER, W.P. WEST, D.G. WHYTE, and R.D. WOOD

JULY 1995

GENERAL ATOMICS

DISCLAIMER

GA–A22091

RECENT DIII–D DIVERTOR RESEARCH

by

S.L. ALLEN,* A.S. BOZEK, N.H. BROOKS, D.A. BUCHENAUER,† K.H. BURRELL, T.N. CARLSTROM, J.W. CUTHBERTSON,‡ J.C. DeBOO, R. ELLIS,* J.C. EVANS,* T.E. EVANS, M.E. FENSTERMACHER,* R.W. GEER,* Ph. GHENDRIH,△ R.J. GROEBNER, D.N. HILL,* D.L. HILLIS,◊ J.T. HOGAN,◊ M.A. HOLLERBACH, K.L. HOLTROP, C.L. HSIEH, A.W. HYATT, G.L. JACKSON, R.A. JAMES,* W.R. JOHNSON, R. JONG,* R. JUNGE, C.C. KLEPPER,◊ C.J. LASNIER,* G.J. LAUGHON, A.W. LEONARD, M.A. MAHDAVI, R. MAINGI,# M.M. MENON,◊ P.K. MIODUSZEWSKI,◊ R.A. MOYER,‡ W.H. MEYER,* D.G. NILSON,* T.H. OSBORNE, D.O. OVERSKEI, L.W. OWEN,◊ T.W. PETRIE, D.A. PHELPS, G.D. PORTER,* M.E. RENSINK,* G.T. SAGER, M.J. SCHAFFER, K.M. SCHAUBEL, T.C. SIMONEN, J.P. SMITH, G.M. STAEBLER, R.D. STAMBAUGH, R.E. STOCKDALE, D.M. THOMAS, M.R. WADE,◊ J.G. WATKINS,† F. WESCHENFELDER,☆ W.P. WEST, D.G. WHYTE,○ and R.D. WOOD*

This is a preprint of an invited paper presented at the 22nd European Conference on Controlled Fusion and Plasma Physics, July 3–7, 1995, in Bournemouth, United Kingdom and to be published in the *PROCEEDINGS*.

Work supported by
the U.S. Department of Energy under
Contract Nos. DE-AC03-89ER51114, W-7405-ENG-48, DE-AC05-84OR21400,
DE-AC04-76DP00789, and Grant Nos. DE-FG03-89ER51121 and DE-FG03-86ER532245

*Lawrence Livermore National Laboratory, Livermore, California.
†Sandia National Laboratories, Albuquerque, New Mexico.
‡University of California at San Diego, La Jolla, California.
△Association EURATOM-CEA, Cadarache, France.
◊Oak Ridge National Laboratory, Oak Ridge, Tennessee.
#Oak Ridge Associated Universities, Oak Ridge, Tennessee.
☆KFA-Jülich, Germany.
○INRS-Energie et Materiaux, Varenne, Quebec, Canada.

GA PROJECT 3466
JULY 1995

GENERAL ATOMICS

Recent DIII-D Divertor Research

S.L. Allen,[1] A.S. Bozek, N.H. Brooks, D.A Buchenauer,[2] K.H. Burrell, T.N. Carlstrom, J.W. Cuthbertson,[3] J.C. Deboo, R. Ellis,[1] J.C. Evans,[1] T.E. Evans, M.E. Fenstermacher,[1] R.W. Geer,[1] Ph. Ghendrih,[4] R.J. Groebner, D.N. Hill, D.L. Hillis,[5] J.T. Hogan,[5] M.A. Hollerbach, K.L. Holtrop, C.L. Hsieh, A.W. Hyatt, G.L. Jackson, R.A. James,[1] W.R. Johnson, R. Jong,[1] R. Junge, C.C. Klepper,[5] C.J. Lasnier,[1] G.J. Laughon, A.W. Leonard, M.A. Mahdavi, R. Maingi,[6] M.M. Menon,[5] P.K. Mioduszewski,[5] R.A. Moyer,[3] W.H. Meyer,[1] D.G. Nilson,[1] T.H. Osborne, D.O. Overskei, L.W. Owen,[5] T.W. Petrie, D.A. Phelps, G.D. Porter,[1] M.E. Rensink,[1] G.T. Sager, M.J. Schaffer, K.M. Schaubel, T.C. Simonen, J.P. Smith, G.M. Staebler, R.D. Stambaugh, R.E. Stockdale, D.M. Thomas, M.R. Wade,[5] J.G. Watkins,[2] F. Weschenfelder,[7] W.P. West, D.G. Whyte,[2] and R.D. Wood[1]

General Atomics, P.O. Box 85608, San Diego, CA 92186-9784
[1]Lawrence Livermore National Laboratory, P.O. Box 808, Livermore, CA
[2]Sandia National Laboratories, P.O. Box 5800, Albuquerque, NM.
[3]University of California at San Diego, Physics Department, La Jolla, CA
[4]Association EURATOM-CEA, Cadarache, France
[5]Oak Ridge National Laboratory, P.O. Box 2009, Oak Ridge, TN
[6]Oak Ridge Associated Universities
[7]KFA-Jülich, Germany
[8]INRS-Energie et Materiaux, Varenne, Quebec, Canada

Abstract. DIII–D currently operates with a single- or double-null open divertor and graphite walls. Active particle control with a divertor cryopump has demonstrated density control, efficient helium exhaust, and reduction of the inventory of particles in the wall. Gas puffing of D_2 and impurities has demonstrated reduction of the peak divertor heat flux by factors of 3–5 by radiation. A combination of active cryopumping and feedback-controlled D_2 gas puffing has produced similar divertor heat flux reduction with density control. Experiments with neon puffing have shown that the radiation is equally-divided between a localized zone near the X-point and a mantle around the plasma core. The density in these experiments has also been controlled with cryopumping. These experimental results combined with modeling were used to develop the new Radiative Divertor for DIII–D. This is a double-null slot divertor with four cryopumps to provide particle control and neutral shielding for high-triangularity advanced tokamak discharges. UEDGE and DEGAS simulations, benchmarked to experimental data, have been used to optimize the design.

1. Introduction

The ultimate goal of the DIII–D divertor research program is to develop particle and power control schemes for tokamaks. This research includes both experiments and detailed modeling of the divertor and scrape-off layer (SOL) plasmas. We are interested in divertor solutions for single-null plasma shapes (e.g., ITER) and in a divertor for an "Advanced Tokamak" (AT), which operates at high β and high τ_E, with a high bootstrap current fraction (Taylor 1994). The AT configuration allows several improvements in reactor concepts (Kikuchi 1993), including significant reductions in size, which in turn lead to a reduced net cost of electricity. Advanced Tokamak operation requires strong plasma shaping, with high triangularity (δ) (Taylor 1993, Lazarus 1994, Osborne 1994), high elongation (κ), and a double-null diverted plasma. Real-time control of the plasma current

profile is also required, which in turn requires active density control for efficient non-inductive current drive.

The present DIII–D machine (Stambaugh 1994a) has an open single or double-null divertor with good diagnostic access; graphite tiles are used for nearly all of the plasma-facing surfaces (Jackson 1995). This geometry is very flexible as it allows operation with single-null (SN) divertors, double-null (DN) divertors, and a variety of plasma shapes, with a wide range of δ (< 0.9) and κ (< 2.2). Efficient wall conditioning, including high-temperature baking (~350°C), boronization, and helium glow discharge cleaning (Jackson 1990, Jackson 1995) are used and rapid recovery is achieved after construction vents (VH–mode in 1–2 weeks) and disruptions (often the next shot). A divertor cryopump (Menon 1992, Smith 1992, Schaubel 1993) and a bias electrode (Schaffer 1992a, Schaffer 1992b) provide active pumping at the outer strike point for lower-single-null, modest triangularity plasmas (δ~0.5) (Mahdavi 1992, Mahdavi 1995). An extensive set of core and divertor diagnostics provides data that has been compared with computer models of the SOL (Hill 1993, Fenstermacher 1995, Owen 1995). We have performed gas puffing experiments with D_2 and impurities (Petrie 1991, Petrie 1992, Petrie 1995). Significant reductions in the peak divertor heat flux have been achieved, and we are making progress with experiments to control the plasma density at the same time (Hill 1990a, Hill 1994). To provide particle control for AT shapes, we have designed a new divertor which has four cryopumps for density control in high δ plasmas (Allen 1995). Detailed modeling has indicated that the baffles in this configuration will control the core ionization current, which is expected to be important for operation at high τ_E (Stambaugh 1994b). This new, more-closed divertor will not allow the large range of plasma shapes studied in the present DIII–D, and plasma shape data has been used to select the best high-triangularity configuration (Lazarus 1993, Lazarus 1994).

In the next section, we present an overview of results from the current divertor configuration, along with locations of divertor diagnostics. Section 3 describes particle control experiments with active cryopumping and biasing. Section 4 summarizes the gas puffing and pumping results with both D_2 and impurities in low-triangularity single-null plasmas. Section 5 presents gas puffing results in (unpumped) double-null plasma configurations. A description of the new Radiative Divertor is presented in Section 6. The results of model benchmarking and model calculations for this high-triangularity divertor design are discussed in Section 7.

2. Basic Properties of The DIII–D SOL

An extensive set of diagnostics is used on DIII–D to measure core and SOL parameters (Hill 1990b). Several are used for power balance measurements, and we have been able to account for more than 85% of the injected power (Leonard 1995a). As shown in Figure 1, a 48-channel bolometer array measures radiation along chords that pass through the core and divertor plasmas; these data are then inverted to obtain emission profiles. Infrared camera (IRTV) systems measure the surface temperature (from which the heat flux is derived) at six locations: 1–2) the lower divertor at two toroidal locations, 3) the lower divertor including the pump entrance, 4) the upper divertor, 5) the lower center-post, and 6) the upper centerpost. Several instruments measure visible plasma emissions, including a multi-chord divertor spectrometer, two cameras with bandpass filters (one with a tangential view centered on the X-point, and the other with a vertical view of the lower divertor from above), and multiple chords at the plasma midplane. An EUV spectrograph measures impurity emissions along a tangential midplane chord.

The radiation profiles from the inverted bolometer data for an ELMing H–mode shot (82151) are shown in Figure 2(a). The radiation is concentrated on the inner divertor leg

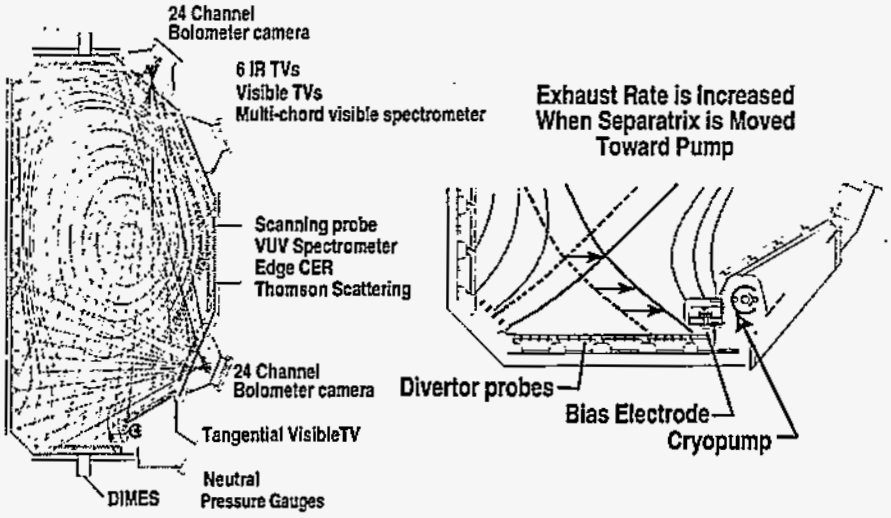

Figure 1. The diagnostic layout for the lower divertor in DIII–D

$$\left(\frac{P_{rad}^{in}}{P_{input}} : \frac{P_{rad}^{out}}{P_{input}} \sim \frac{23\%}{7\%} \sim \frac{3.2}{1} \right) ,$$

so that the heat flux profiles measured by the IRTV's at the lower divertor plate are asymmetric

$$\left(\frac{P_{div}^{in}}{P_{input}} : \frac{P_{div}^{out}}{P_{input}} \sim \frac{4\%}{41\%} \sim \frac{1}{10} \right) .$$

The remainder of the power is heat flux on the inner wall (~11 %) and core radiation (~16%). The in-out sense of the radiation asymmetry (and therefore the in-out heat flux asymmetry) is often due to factors other than the direction of the ∇B drift (i.e., changing the ∇B direction does not necessarily reverse the asymmetry). The electron density does influence the asymmetry, however, as we observe that as the density is lowered with cryo-pumping from ~5-7 × 10^{19} m^{-3} to 3 × 10^{19} m^{-3}, the heat flux profile becomes more symmetric (Maingi 1995c). To date, we have compared the UEDGE calculation of the divertor heat flux with the measurements of the outer heat flux, as the code was not able to calculate the two-dimensional distribution of the impurity radiation. The midplane Te, T_i, and n_e profiles fit with D~0.2 and χ~0.15–0.3,

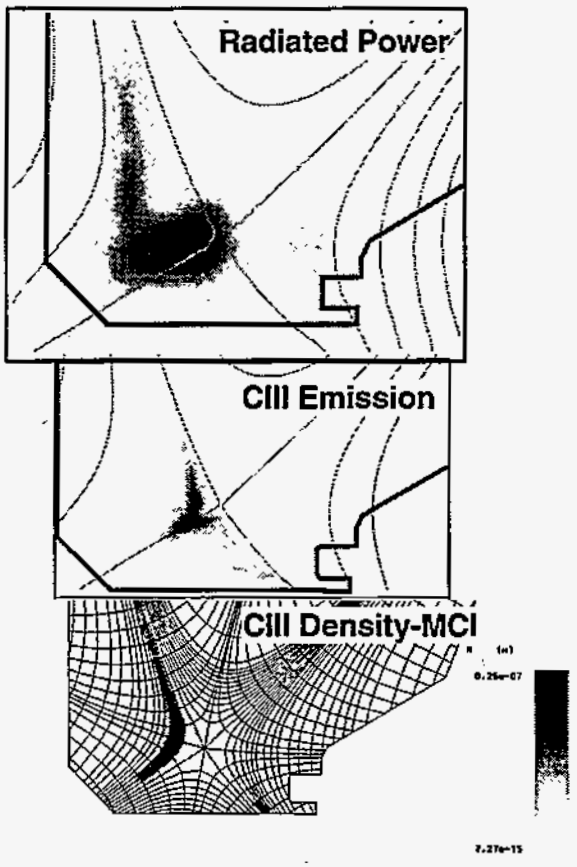

Figure 2. (a – top) The Bolometer inversion shows enhanced inner radiation. The inverted CIII emission from the Tangential TV (b – middle) and the calculated CIII density from MCI (c – bottom) are similar.

calculate the two-dimensional distribution of the impurity radiation. The midplane T_e, T_i, and n_e profiles are fit with D~0.2 and χ~0.15–0.3, and the code calculates the SOL quantities. We usually find at least factor-of-two agreement between UEDGE and the IRTV measurements of the outer heat flux. Recently, the UEDGE code has been upgraded to include multi-species impurity transport, and comparisons of these code results with the data are in progress.

Shown in Figure 2(b) is an inversion from a tangential TV camera with a CIII (4650 Å) filter; note there is good qualitative agreement with the inverted bolometer data, suggesting that a significant portion of the total radiation is due to carbon. We have recently calibrated this system, and plan to obtain calibrated data from carbon and deuterium ionization states. Shown in Figure 2(c) is the result of a calculation of CIII density from the Monte-Carlo Impurity (MCI) transport code (Evans 1995). The UEDGE code was used to calculate the background plasma for the MCI calculation. There is good qualitative agreement with the measured CIII emission in Figure 2(b) (i.e., more density along the inner leg of the divertor). These results, along with H_α measurements, imply that the divertor radiation comes primarily from deuterium and carbon.

Several other diagnostics are used for comparisons with SOL codes and to study the plasma pressure in the SOL. A multi-chord(36), multiple-pulse (7 lasers at 20 Hz each) Thomson Scattering system (Carlstrom 1992) measures n_e and T_e in the core and SOL near the plasma midplane. As shown in Figure 3, we have studied the SOL density profiles in several operational modes and find a significantly broaded density profile (i.e., an edge plateau) after the ELM in H–mode (Jong 1995). The local density scale length at the separatrix, $L_n = -n_e/(dn_e/dr)$ increases by about a factor of 2 during the ELMing H–mode phase (even after accounting for uncertainties in the separatrix location due to the magnetic reconstruction with EFIT). The plateau formation is also observed after VH–mode termination, as well as in steady-state ELMing H–mode. We have not observed large SOL density enhancements (i.e., the density plateau) in L– or VH–mode plasmas.

The n_e and T_e profiles from the Thomson system, along with T_i profiles from a multi-chord Charge Exchange Recombination (CER) system provide measurements of the plasma pressure at the midplane. An array of 20 domed probes (i.e., extending slightly above the divertor plate surface) (Buchenauer 1990) are used to obtain n_e, T_e, and I_{sat} at the divertor plate. Except in gas puffing experiments (discussed below), we observe pressure balance (within a factor of two) along the field line. We are also adding diagnostics to obtain the variation of n_e and T_e along the field line, particularly from the X-point to the floor. A 250 GHz divertor interferometer measures the line density across the outer leg of the divertor. By sweeping the X-point, we can measure the line-density along the field line. Preliminary measurements indicate a factor of two increase in the line-density between locations ~12 cm and ~2 cm from the floor in a ohmic plasma with an ~20 cm X-point height. We are running UEDGE to compare with these data. In ELMing H–mode operation, the line-density in the outer divertor between ELMs measured with the interferometer agrees with calculations from the UEDGE code to within 20%.

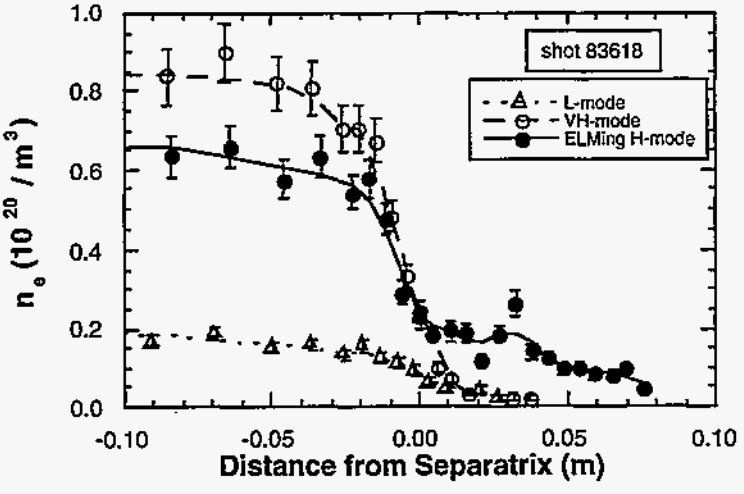

Figure 3. There is an edge density plateau in ELMing H–mode. This is not observed in L–mode or VH–mode.

3. Particle Control With Active Cryopumping

Density control is necessary in an AT to optimize non-inductive current drive for current-profile control. The helium-cooled cryopump shown in Figure 1 has a D_2 pumping speed of 30,000 ℓ/s at 2 mTorr. The pumping rate is varied in a closed feedback loop for density control by moving the outer separatrix toward or away from the pump entrance. Pumping rates during ELMing H–mode were 40 Torr ℓ/s (Mahdavi 1993), which is larger than the beam fueling rate of ~10-20 Torr ℓ/s. The particle balance indicates that the remainder is particle removal from the wall (~50 Torr ℓ per shot, depending on wall conditions (Maingi 1995b) with pumping. The H–mode density could be decreased by over 40%. This feature allowed us to determine that τ_E scales weakly with n_e and nearly linearly with I_p (Schissel 1994). Pumping does not affect τ_E, and the reduction in n_e is accompanied by an increase in T_e, which increases the current-drive efficiency. Previously, reduction of core density was limited by the appearance of locked modes. The installation of a new error field correction coil has enabled operation in the range of $\sim 1 \times 10^{19}$ m^{-3} (La Haye 1995).

Preliminary particle control experiments for AT plasma shapes show promising results. (As seen in Figure 1, the present cryopump is not located for optimum pumping of high confinement, high triangularity, VH–mode plasmas with the X-point near the inner wall.) Preliminary pumping experiments with ELM-free H–modes (in asymmetric double-null plasmas, with lower δ, lower κ to match the pump) have shown that the rate of rise of plasma density after the L-H mode transition was reduced by nearly a factor of 2, from 40–60 Torr ℓ/s to 20–30 Torr ℓ/s (Stambaugh 1994b) with a pumping rate of 13 Torr ℓ/s. In low-δ, (symmetric double-null) reduced-τ_E VH–mode plasmas, pumping rates of 7.5 Torr ℓ/s have been measured. A general trend is that discharges with increased τ_E are accompanied by low neutral pressures.

We have also performed plasma operation with pumping to determine if it can replace He glow discharge cleaning (GDC) between shots on DIII–D (Maingi 1995b, Maingi 1995a). This is important for machines with superconducting magnets that provide steady-state magnetic fields (e.g., TPX, although ECDC could also be used). As shown in Figure 4, several shots without GDC and the pump warm were used to load the wall to ~1250 Torr ℓ. The variation in the loading per shot was due to an increase in the programmed line-average density (e.g., shot 83751). At the end of this sequence, good plasma startup conditions (burnout of impurities) could not be obtained even though no gas was puffed into the discharge. The pump was then turned on and normal plasma operation resumed (shot 83757 in Figure 4). The wall loading was reduced by plasma operation and pumping. Again, the variation in the removal rate was due to variations in the programmed core-plasma density. High-density H–mode discharges were programmed after the pump was cooled, which required additional gas input. Subsequent shots were programmed for lower density (e.g., shot 83761) and a greater reduction in wall loading was achieved. While this technique clearly demonstrates a control of the wall inventory with pumping, it has not been tested with recovery from disruptions. The normal DIII–D case is that we can recover between shots with He GDC.

As shown in Figure 1, a bias electrode and insulator form the entrance to the pump. The bias system both drives a current in the SOL (14 kA measured, 20 kA possible) and can generate E×B drifts to enhance particle exhaust rates (Schaffer 1992a, Schaffer 1993, Staebler 1995). We have shown that the exhaust rate increases as the separatrix is swept toward the pump without biasing (Menon 1994, Maingi 1995c). A –200 V bias increases the

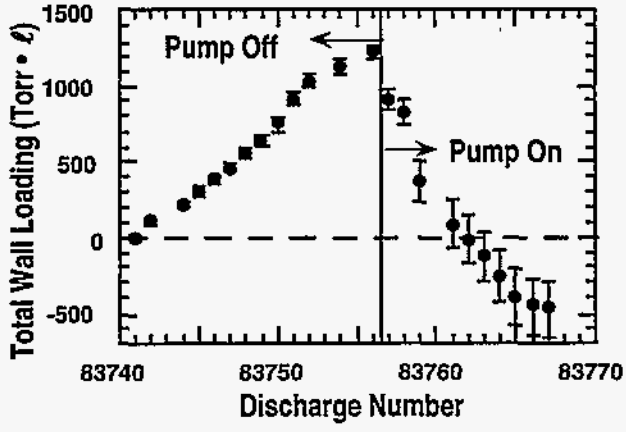

Figure 4. Plasma pumping decreases the particle inventory of the wall.

achievable exhaust rate by a factor of 2 and decreases the sensitivity of the exhaust rate to the separatrix strike point location. Also shown in Figure 5, we observe a strong dependence of the exhaust rate (y) with electron density, both with and without bias (Schaffer 1993, Schaffer 1995b). These results show that biasing is a useful tool, providing operational flexibility in a divertor design.

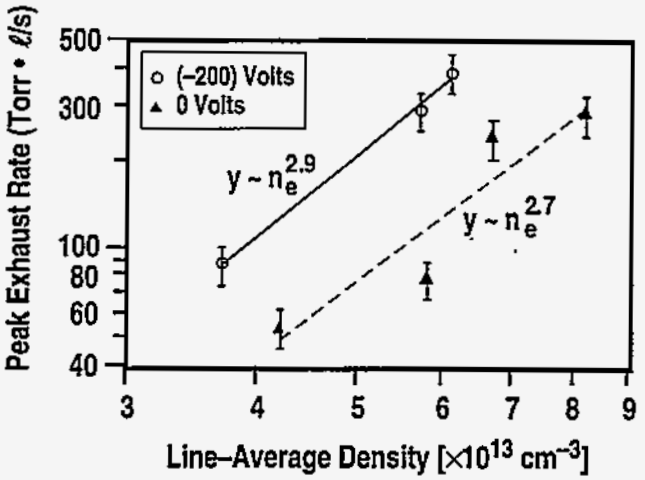

Figure 5. The particle exhaust by the pump is increased by a negative bias. The exhaust rate is a strong function of density.

The cryopump can also pump helium when a 1.5 μm layer of argon is deposited on the pump. The pumping speed for He immediately after depositing the argon layer was 18,000 ℓ/s, which decreased during the discharge as the argon layer was covered with D_2. Core He transport and exhaust were studied using He gas puffing and energetic He injected by neutral beams (Wade 1994, Wade 1995). It was found that the exhaust rate was not limited by the core He transport, but by the exhaust efficiency of the pump. The ratio of the effective particle confinement time to the energy confinement time, τ^*_{He}/τ_E was ~11, which is within the ITER requirements (7–11). It is also observed from perturbative transport studies that no preferential peaking of He occurs, i.e., D_{He}/χ_{eff} ~1 for L–, H–, and VH–modes of operation.

4. Simultaneous Control Of Divertor Heat Flux And Core Particle Flux

We have demonstrated previously the reduction in the peak heat flux in H–mode plasmas with both D_2, neon, argon, and nitrogen puffing (Allen 1995, Petrie 1995, Schaffer 1995a) Recently, we have added pumping to these experiments to control the density (i.e., during D_2 puffing) and to control or entrain impurities in the divertor (during neon or argon injection with pumping and with or without D_2 injection).

4.1 Deuterium Puffing with Pumping

Previous unpumped D_2 gas puffing experiments have injected ~50–150 Torr ℓ/s either near the plasma midplane or in the divertor. After a delay of typically several hundred ms, the peak heat flux drops by a factor of 3–5. Compared to the non-puffing case shown in Figure 2, the bolometer inversion shows an increase in radiation from the X-point towards the outer strike point (Leonard 1995b). The vertical interferometer chord that passes through this region increases relative to the chord that passes outside of this region, indicating that at least part of the increase in radiation is due to a local increase in the divertor density. We find that the peak heat flux reduction is independent of the input power. Without pumping, the density usually rises slowly throughout the discharge, and we can operate at 0.6–0.8 of the Greenwald density limit (Petrie 1995).

Another overall feature of D_2 puffing is a dramatic decrease in the plasma pressure measured at the divertor plate near the separatrix $\mathcal{P}_{div}(s)$ compared to the plasma midplane $\mathcal{P}_{mid}(s)$ that accompanies the decrease in the peak divertor heat flux. The plasma pressure at the plate $\mathcal{P}_{div}(s)$ is measured with Langmuir probes, and we assume the ion and electron pressures are equal. The midplane plasma pressure $\mathcal{P}_{mid}(s)$ uses n_e and T_e measured by Thomson Scattering, T_i measured by CER and we assume $n_e \sim n_i$. The plasma pressure ratio $\mathcal{P}_{mid}(s)/\mathcal{P}_{div}(s)$ increases from ~2 (before puffing, pump cold, small exhaust) to ~40

(with puffing and exhaust), a factor of 20. For some flux lines outside of the separatrix ($r > s$), we observe that $\mathcal{P}_{mid}(r > s)/\mathcal{P}_{div}(r > s) \sim 0.5–1$, suggesting radial transfer of momentum. Models support this observation and suggest charge-exchange with neutrals as the mechanism (Ghendrih 1994). This Partially-Detached Divertor (PDD) (i.e., detachment primarily near the separatrix) with reduced peak divertor heat flux is a stable configuration, and can be maintained without feedback.

We have started experiments to combine divertor heat flux reduction and density control. We have sustained a PDD discharge (Hill 1994) with particle exhaust for the duration of the D_2 gas pulse, ~2 s. The exhaust rate (180–240 Torr ℓ/s) nearly matched the gas fueling rate (210 Torr ℓ/s, the beam input is substantially smaller, ~10–20 Torr ℓ/s), so the core plasma density was nearly constant. This was a high-quality ELMing H–mode [$\tau_E \sim 2 \times \tau$(ITER89)], with a very modest decrease in τ_E due to the gas puff. The inverted bolometer profile and CIII profile are shown in Figure 6. The radiation and CIII emission now extend from the X-point towards the outer strike point. These profiles are similar to the unpumped case (Leonard 1995b). While it should be noted that these are currently qualitative, preliminary comparisons, there do not seem to be any dramatic changes in the C III spatial distribution due to the gas puffing and pumping in these discharges.

We have further refined the D_2 gas puffing technique by controlling the gas flow with a divertor photodiode signal in a feedback loop. Shown in Figure 7 is a comparison between an unpumped PDD discharge (shot 79342) and a pumped discharge with closed-loop feedback (shot 83695). The gas puff was slowly ramped in shot 83695, and the D_α photodiode was used to sense the transition to the PDD mode (i.e., a sharp increase in the signal above a pre-set level at ~3 s). At this time, the gas flow was clamped to maintain the mode. Note that the pumped shot has lower core density, a similar peak heat flux reduction, and very good H–mode confinement, with $\tau_E \sim 2 \times \tau$ (ITER-89P). Shot 83695 did not use all of the available pumping capability, and future experiments are planned to investigate the effects of exhaust rate on PDD plasmas.

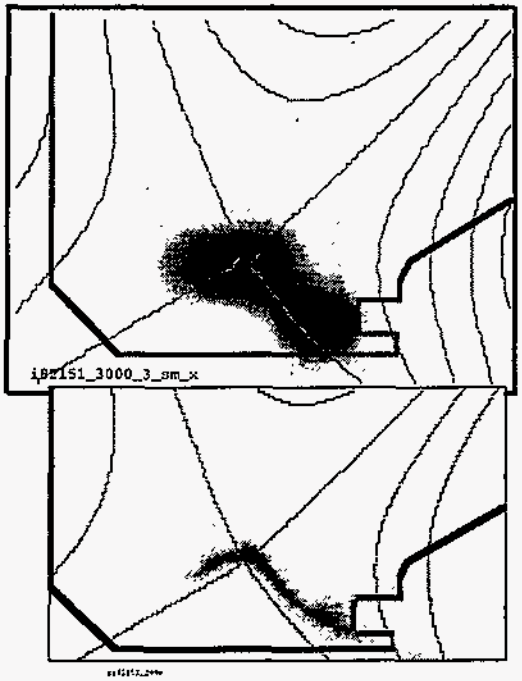

Figure 6. The radiated power from the bolometer (top) and the inverted CIII emission from the tangential TV. These data are from a shot with deuterium injection and pumping (82151).

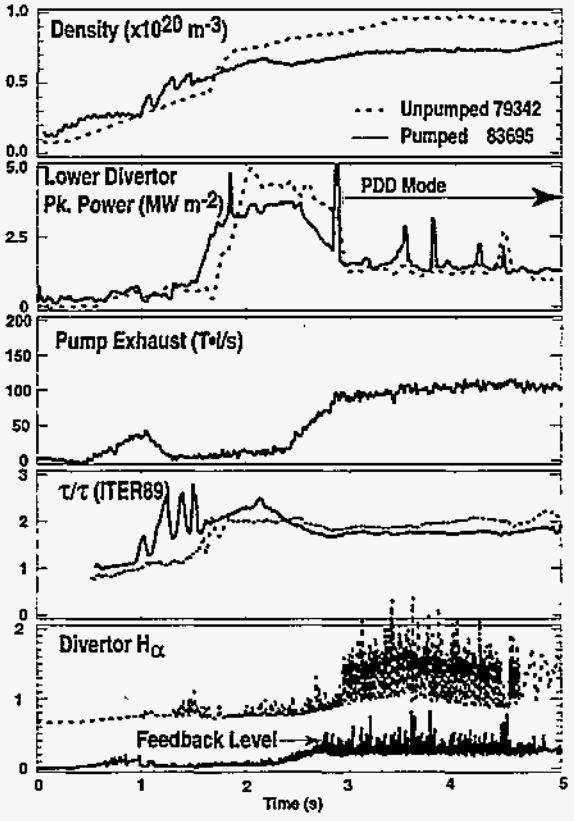

Figure 7. The pumped (solid) discharge with D_2 puffing has a lower core density than the unpumped (dashed). The gas flow was controlled by the photodiode signal.

4.2 Impurity Puffing with Pumping

We have also studied the effects of impurity puffing on the SOL and divertor plasmas. As shown in Figure 8 (dashed lines), a short (~100 ms) puff of neon at ~15 Torr ℓ/s below the X-point causes an immediate reduction in the divertor heat flux by a factor of 3–5. The bolometer data shows that approximately half of the radiation is in a mantle around the plasma core (Allen 1995, Leonard 1995a), and the balance is concentrated in a region near the X-point. The radiative mantle reduces the power flow to the SOL, reducing T_e inside of the separatrix. Unlike the D_2 puffing case, the data from the vertical interferometer chords indicate that the radiation zone near the X-point is not a region of high n_e. The plasma pressure ratio at the separatrix $\mathcal{P}_{mid}(s)/\mathcal{P}_{div}(s)$ is about 5 with neon injection. So far, we have not been able to preferentially concentrate the neon in the divertor, as >25% of the injected neon reaches the core.

We have also performed experiments with impurity puffing in the divertor, D_2 puffing near the midplane, and pumping. The (trace) core argon concentration was reduced by a factor of 20 with a midplane D_2 gas flow of 200 Torr ℓ /s, compared to the case without gas flow (Schaffer 1995a). Puffing may increase the ion flow towards the divertor and increase the frictional forces on impurites in the divertor. In Figure 8 (solid lines) a case of neon injection with pumping is presented. Note that the core electron density and the core neon concentration are less for the pumped case. The confinement is degraded with this amount of neon, although τ/τ(ITER-89) is still ~1.6–1.8. Toward the end of the discharge, the neon injection has a strong effect on ELMs; we have seen reductions of the ELM frequency of a factor of 10. ASDEX-Upgrade has shown that careful balancing of neon, D_2 flow, and pumping are required to maintain a particular ELM condition (Kallenbach 1994, Kallenbach 1995).

5. Double-Null Divertor Physics

As discussed above, highly-shaped DN plasma shapes are an important ingredient in high-confinement AT discharges. Another feature of DN operation is the additional heat flux dispersal over two divertor plates. We have found that by carefully controlling the plasma equilibrium, we can control the heat flux sharing between the upper and lower divertor. During a discharge, we varied the fieldline distance between the lower and upper separatrix measured at the midplane. The distribution of the heat flux between the lower and upper divertor plates varied accordingly (Figure 9), and a slight magnetic imbalance was required to balance the heat flux.

Bolometer inversions of double-null discharges (ELMing H–mode) show a concentrated radiation zone near the outer strike point at both the upper and lower divertor plates. When neon is puffed, a mantle around the core is formed, and the heat flux to the divertor plate is reduced. We have observed a reduction in the peak heat flux of a factor of 3–5. Both the upper and lower heat flux are reduced with gas puffing.

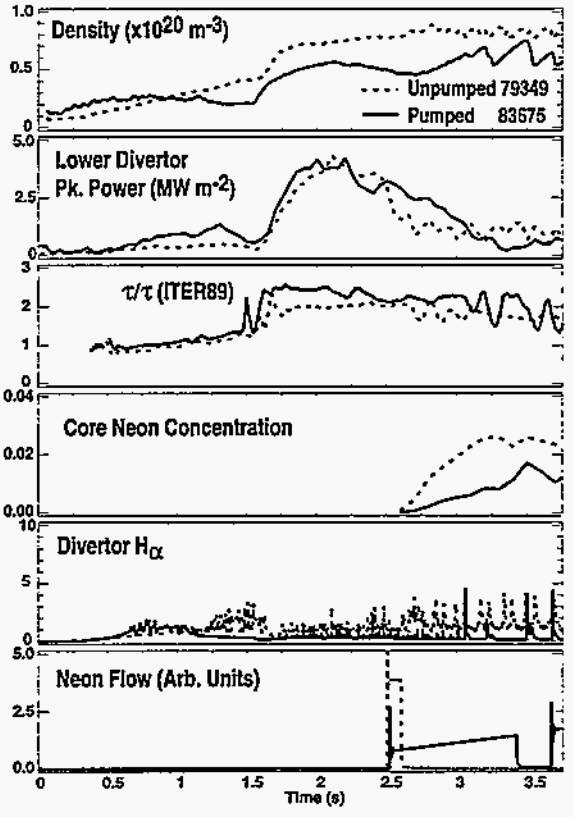

Figure 8. The pumped (solid) discharge has a lower density and lower neon concentration for a similar heat flux reduction

6. The Radiative Divertor In DIII–D

Experimental results and computer models have been used to design a new divertor for DIII–D, called the Radiative Divertor. This installation will provide an important new test-bed for divertor physics and will provide particle control for DN, high-triangularity AT shapes. The Radiative Divertor also allows operation with SN plasma shapes. The main features of the design are shown in Figure 10. Four cryopumps, similar to the existing cryopump, will be installed and can be individually controlled to test several pumping configurations. The design will allow low-current biasing at the outer divertor strike point. A flexible gas injection system will be used to study impurity entrainment issues.

The divertor wall geometry is very flexible and can be changed by installing a set of graphite tiles with the desired shape (e.g., a different slot width or slot wall contour). With the quick-recovery wall-conditioning techniques used on DIII–D, we estimate this could be accomplished in ~1 month, and we anticipate studying two geometries per year. The length of the baffled region can be changed by lengthening the graphite tile supports and we have design cases of 23 cm, 33 cm, and 43 cm lengths (X–point to outer strike point). The length change requires more modifications, so it is anticipated that this will occur during annual maintenance vents. The Radiative Divertor is scheduled for completion in December of 1996.

The Radiative Divertor will also include a test of a low-activation Vanadium alloy (4% Cr, 4% Ti, Vn). The supports for the graphite plates in the upper divertor will be made from this material. This installation will provide an important test of this alloy in a tokamak environment, and will address several issues: fabrication of basic products (plates, etc.), impurity control in welds, and behavior of the alloy in a tokamak environment (impurities and hydrogen at bakeout temperatures of ~350°C).

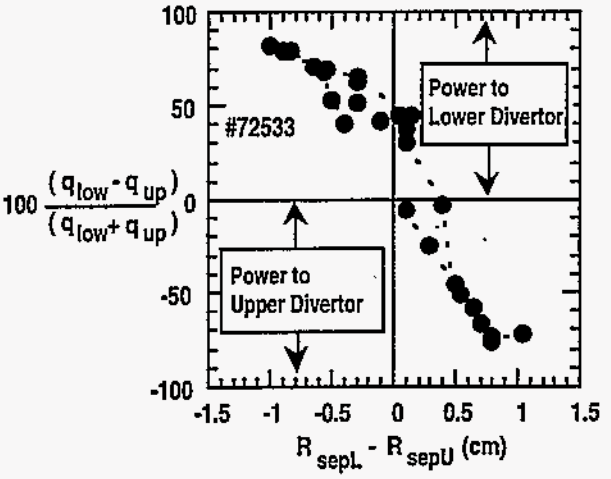

Figure 9. The difference over the sum of the measured upper and lower heat flux vs. the fieldline distance between the lower and upper separatrix measured at the midplane. Magnetic imbalance is required for a balanced heat flux.

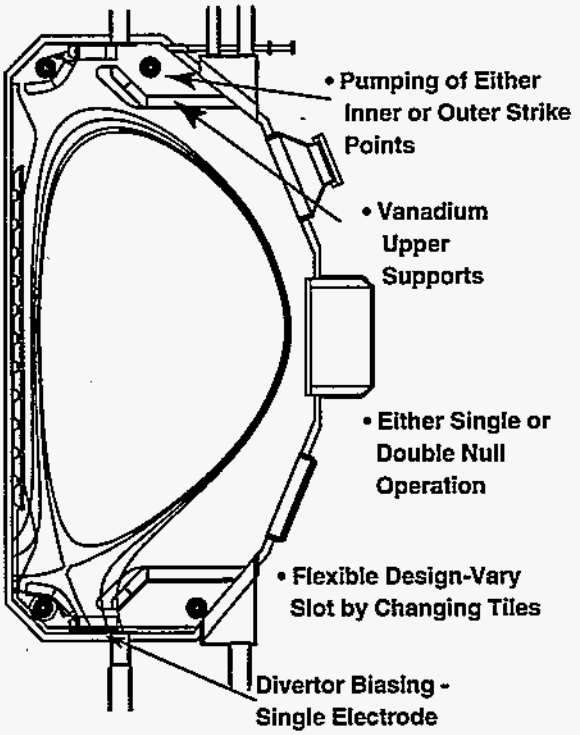

Figure. 10. Overview of the Radiative Divertor for DIII–D.

7. Edge Modeling: Comparison With Data And Divertor Design

A detailed description of the UEDGE fluid modeling of the DIII–D edge plasma is presented elsewhere (Fenstermacher 1995, Porter 1995). Briefly, the UEDGE model uses

the measured temperature and density profiles at the plasma midplane as inputs, and calculates the edge plasma quantities in the SOL and divertor. UEDGE has been compared with experimental data at the divertor plate (e.g., the measured heat flux) and good agrement has been obtained (the peak heat flux agrees to better than a factor of 2, the total agrees within 30%). UEDGE fluid equations are solved on a non-orthogonal grid, and several impurity transport packages are currently being added. A generalized neutrals model capable of simulating momentum removal is also in development.

We have used computer models to guide the design of the new divertor for DIII–D. While these calculations are for the specific case of DIII–D, they demonstrate several general divertor-design principles. The nonorthogonal calculational grid of the UEDGE code was very important for these studies, as we were concerned with the details of the recycling from the specific divertor shapes. The DEGAS Monte-Carlo neutrals code was then used to calculate the neutral distribution on the UEDGE plasma solution. An example of these calculations in shown in Figure 11, where the models calculated the amount of ionization current into the plasma core as a function of the position of the outer divertor baffle. For this baffle shape, the greatest reduction in core ionization was calculated for the case when the innermost projection of the outer baffle (the "nose") was located on the 1.5 cm SOL field line (measured at the midplane). While these were "single pass" calculations with UEDGE and DEGAS, we observed a similar dependence using the simplified neutrals model in UEDGE. Self consistent calculations with the faster DEGAS-II code are in progress.

We examined the poloidal distribution of the core ionization current to understand the above results and determine if further optimization of the baffle shape was possible (using core ionization as the figure of merit). In the case of the outer open baffle, the peak in the ionization source profile entering the core is near the outer midplane, indicating neutral leakage between the SOL and the baffle. As the outer baffle nose is moved inward, the peak in the core source distribution moves closer to the X–point, indicating that recycling off of the upper surface of the baffle is the dominant source. The minimum core ionization discussed above is the best compromise between a open baffle that leaks and a narrow baffle that produces recycling sources near the core plasma. We have also varied the angle of the baffle in the model, and the optimum angle is used in the present design. These calculations also highlight the need for an angled baffle with respect to the flux surfaces, so that neutrals recycling on the baffle are directed towards the separatrix where the ionization mean free path is short. Other calculations showed that the inner baffle also reduced the ionization current; we are presently optimizing its shape.

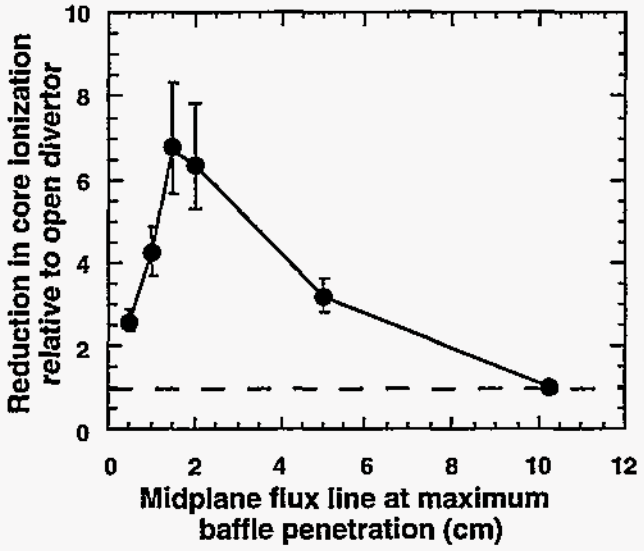

Figure 11. A UEDGE-DEGAS calculation shows the optimum baffle width is 1.5 cm. The figure of merit is the reduction in the core ionization relative to an open divertor.

Simulations with impurity transport models are also being tested. The UEDGE code has several impurity models: a) a uniform impurity concentration, with noncoronal radiation, b) an average-ion model treatment of impurity transport, and c) a full, multi-species treatment of impurity transport. These calculations will be important both for comparisons with experimental data (e.g., Figure 2), and for predictions of behavior with new divertor structures.

8. Summary

We have presented here the experiments and modeling on DIII–D to develop single and double-null divertor solutions. In the current open, single-null DIII–D divertor, we account for over 85% percent of the input power, and observe a "natural" inner radiative divertor, where in-out radiation asymmetry causes a marked asymmetry in the divertor heat flux. Efficient pumping with a divertor cryopump allowed density control and helium exhaust. D_2 puffing with cryopumping and feedback has enabled us to reduce the divertor heat flux and simultaneously control the core density. The radiation becomes more concentrated in the outer divertor leg, and the ratio of the midplane to plate plasma pressure drops by about a factor of 20. With neon injection, we form a radiating mantle, and the midplane to plate pressure ratio is about 5. Preliminary density control experiments have been carried out with neon. Double-null experiments have shown similar heat flux reductions, and require a slightly unbalanced magnetic configuration to obtain a blanced heat flux.

A new Radiative Divertor is being constructed for DIII–D. The design is flexible, as the baffle width and height can be easily varied. The benchmarked UEDGE and DEGAS models have been used to calculate the reduction in the core ionization with divertor baffles; a factor of over 7 is obtained. The upper divertor support structure is constructed of low-activation vanadium. The Radiative Divertor is scheduled for operation late in 1996.

Acknowledgments

This work has been a group effort involving the experimental, theoretical, technical, operations, and modeling parts of the DIII–D Team. This is a report of work supported by the U.S. Department of Energy under Contract Nos. W-7405-ENG-48, DE-AC03-89ER51114 and DE-AC05-84OR21400, DEAC04-76DP00789, and Grant Nos. DE-FG03-89ER51121 and DE-FG03-86ER532245.

References

Allen S L *et al.* 1995 *J. Nucl. Mater.* **220-222** 336
Buchenauer D *et al.* 1990 *Rev. Sci. Instrum.* **61** 2873
Carlstrom T N *et al.* 1992 *Rev. Sci. Instrum.* **63** 4901
Evans T E *et al.* 1995 "Monte-Carlo Impurity Transport Simulations in the Edge of the DIII–D Tokamak Using the MCI Code," to be published in *Tenth Int. Conf. on Stellarators, Madrid, Spain*, General Atomics Report GA-A22064
Fenstermacher M E *et al.* 1995 *J. Nucl. Mater.* **220-222** 330
Ghendrih Ph 1994 *Physics of Plasmas* **1** 1929
Hill D N *et al.* 1990a *Plasma Physics and Controlled Nuclear Fusion Research 1990 Washington* (International Atomic Energy Agency, Vienna) Vol. 3 p 487
Hill D N *et al.* 1990b *Rev. Sci. Instrum.* **61** 3548
Hill D N *et al.* 1993 *Proc. of the 20th Euro. Conf. on Contr. Fusion and Plasma Physics* (European Physical Society, Petit-Lancy, Switzerland, Lisboa, Portugal) Vol. 17C p 643
Hill D N *et al.* 1994 " Divertor Research on the DIII–D Tokamak." to be published in *Plasma Physics and Controlled Nuclear Fusion 1994 Madrid*
Jackson G L *et al.* 1990 *Nucl. Fuion* **30** 2305
Jackson G L *et al.* 1995 *J. Nucl. Mater.* **220-222** 173
Jong R *et al.* 1995 "Properties of DIII–D Edge Plasmas," to be submitted to *Nucl. Fusion*
Kallenbach A *et al* 1994 "Radiating Boundary in ASDEX Upgrade Divertor Discharges," to be published in *Plasma Physics and Controlled Nuclear Fusion 1994 Madrid*
Kallenbach A *et al* 1995 "H–mode Discharges with Feedback-Controlled Radiative Boundary in the ASDEX Upgrade Tokamak," to be published in *Nucl.. Fusion*
Kikuchi M *et al* 1993 *Plasma Phys. Contr. Fusion* **35** B39
LaHaye R 1995 to be published in these proceedings
Lazarus E A *et al* 1993 *Bull. Am. Phys. Soc.* **38** 1936

Lazarus E A *et al* 1994 to be published in *Plasma Physics and Controlled Nuclear Fusion 1994 Madrid*
Leonard A W *et al* 1995a *J. Nucl. Mater.* **220-222** 325
Leonard A W *et al* 1995b "Radiation Distributions in Detached Divertor Operation on DIII–D," to be published in these proceedings
Mahdavi M A *et al* 1992 *Plasma Physics and Controlled Nuclear Fusion 1992 Würzburg* (International Atomic Energy Agency, Vienna) Vol. 1 p 335
Mahdavi M A *et al* 1993 *Proc. of 20th Euro. Conf. on Contr. Nucl. Fusion and Plasma Physics* (European Physical Society, Petit-Lancy, Switzerland, Lisboa, Portugal) Vol. 17C p 647
Mahdavi M A *et al* 1995 *J. Nucl. Mater.* **220-222** 13
Maingi R *et al* 1995a "Control of Wall Particle Inventory with Divertor Pumping on DIII–D," submitted to *Nucl. Fusion*
Maingi R *et al* 1995b "Divertor Particle Exhaust and Wall Inventory on DIII–D," to be published in these proceedings
Maingi R *et al* 1995c *J. Nucl. Mater.* **220-222** 320
Menon M M *et al* 1992 *Fusion Technol.* **22** 356
Menon M M *et al* 1994 "Particle Exhaust Characteristics of an In-Vessel Cryopump Used in DIII–D Diverted Plasmas," to be published in *Fusion Technology*
Osborne T H *et al* 1994 *Plasma Physics and Controlled Nuclear Fusion* **36-7** A237
Owen L W *et al* 1995 *J. Nucl. Mater.* **220-222** 315
Petrie T W *et al* 1991 *Proc. of 18th Euro. Conf. on Contr. Fusion and Plasma Physics* (European Physical Society, Petit-Lancy, Switzerland, Berlin, Germany) Vol. 3 p 237
Petrie T W *et al* 1992 *J. Nucl. Mater.* **196-198** 848
Petrie T W *et al* 1995 "Radiative Divertor Experiments in DIII–D with Deuterium Injection," submitted to *Nucl. Fusion* General Atomics Report GA-A21879
Porter G D *et al* 1995 "Analysis of SOL and Divertor Behavior in DIII–D," to be published in these proceedings
Schaffer M J *et al* 1992a *Nucl. Fusion* **32** 855
Schaffer M J *et al* 1992b *Plasma Physics and Controlled Nuclear Fusion 1992 Würzburg* (International Atomic Energy Agency, Vienna) Vol. 1 p 299
Schaffer M J *et al* 1993 *Proc. IAEA Technical Committe Meeting on Tokamak Plasma Biasing* (IAEA, Vienna) Vol. p 340
Schaffer M J *et al* 1995a "Impurity Reduction During 'Puff and Pump' Experiments on DIII–D," to be published in *Nucl. Fusion*
Schaffer M J *et al* 1995b "Increased Divertor Exhaust by Electrical Bias in DIII–D," submitted to *Nucl. Fusion,* General Atomics Report GA-A21878
Schaubel K *et al* 1993 *Proc. of 1993 Cryogenic Engineering Conference* , July 12–16, 1993) Vol.
Schissel D P *et al* 1994 *Nucl. Fusion* **34** 1994
Smith J P *et al* 1992 *Fusion Technol.* **21** 1638
Staebler G M *et al* 1995 *J. Nucl. Mater.* **220-222** 158
Stambaugh R D *et al* 1994a "DIII–D Program Overview," to be published in *Plasma Physics and Controlled Nuclear Fusion 1994 Madrid*
Stambaugh R D *et al* 1994b *Plasma Physics and Controlled Fusion* **36-7A** 249
Taylor T S *et al* 1993 *Plasma Physics and Controlled Nuclear Fusion 1992 Würzburg* (International Atomic Energy Agency, Vienna) Vol. 1 p.111
Taylor T S *et al* 1994 *Plasma Physics and Controlled Fusion* **36** B229
Wade M R, et al. 1994 Helium Transport and Exhaust Studies in Enhanced Confinement Regimes in DIII–D, to be published in *Physics of Plasmas*, General Atomics Report GA-A21905.
Wade M R, et al. 1995 *Phys. Rev. Lett.* **74** 2702

GENERAL ATOMICS

P. O. BOX 85608 SAN DIEGO, CA 92186-9784 (619) 455-3000